Reference: *Biol. Bull.* 198: 50–66. (February 2000)

Nucleation and Growth of Calcite on Native *Versus* Pyrolyzed Oyster Shell Folia

C. S. SIKES[1,*], A. P. WHEELER[2], A. WIERZBICKI[3], A. S. MOUNT[2], AND R. M. DILLAMAN[4]

[1]*The Mineralization Center, Department of Biological Sciences;* [2]*Department of Biological Sciences, Clemson University, Clemson, South Carolina 29634-1903;* [3]*Department of Chemistry, University of South Alabama, Mobile, Alabama 36688; and* [4]*Department of Biological Sciences, University of North Carolina at Wilmington, Wilmington, North Carolina 28403-3297*

Abstract. The thin sheets of calcite, termed folia, that make up much of the shell of an oyster are covered by a layer of discrete globules that has been proposed to consist of agglomerations of protein and mineral. Foliar fragments, treated at 475°C for 36 h to remove organic matter, were imaged by atomic force microscopy (AFM) as crystals grew on the foliar surfaces in artificial seawater at calcite supersaturations up to 52-fold. Crystals were also viewed later by scanning electron microscopy. After pyrolysis, the foliar globules persisted only as fragile remnants that were quickly washed away during AFM imaging, revealing an underlying morphology on the foliar laths of a tightly packed continuum of nanometer-scale protrusions. At intermediate supersaturations, crystal formation was seen immediately almost everywhere on these surfaces, each crystal having the same distinctive shape and orientation, even at the outset with crystals as small as a few nanometers. In contrast, nucleation did not occur readily on non-pyrolyzed foliar surfaces, and the crystals that did grow, although slowly at intermediate supersaturations, had irregular shapes. Possible crystallographic features of foliar laths are considered on the basis of the morphology of ectopic crystals and the atomic patterns of various surfaces. A model for foliar lath formation is presented that includes cycles of pulsed secretion of shell protein, removal of the protein from the mineralizing solution upon binding to mineral, and mineral growth at relatively high supersaturation over a time frame of about 1 h for each turn of the cycle.

Received 20 January 1999, accepted 16 November 1999.

* To whom correspondence should be addressed. E-mail: ssikes@usamail.usouthal.edu

Introduction

The mineral of most molluscan shells is $CaCO_3$ that routinely contains less than a few percents and often less than 1% by weight of the shell as organic material, mostly protein. One objective of shell research is to understand how the shell is put together, particularly the relationships between the mineral and the organic components. The intrinsic appeal of exquisite biominerals like shells has been advanced in recent years by an appreciation of the material properties of the structures (Heuer *et al.*, 1992; Sarikaya *et al.*, 1995; Mann, 1996; Stupp and Braun, 1997; Weiner and Addadi, 1997). A variety of studies have shown that biological composites like shell have particularly favorable properties, including increased durability and resistance to fracture. Such properties are considered to result from the interplay of the organic and inorganic components, even though the organic content is quite low by composite-materials standards.

In the case of the oyster shell, which is composed of calcite and is representative of many kinds of molluscan shell, the mineral even within a few millimeters of the forming edge is formed into layers of thin sheets, termed folia (Tsujii *et al.*, 1958; Carriker and Palmer, 1979; Carriker *et al.*, 1980). The foliar layers form the bulk of the shell. Each foliar sheet is subdivided into units termed laths, with each sheet just one lath unit of up to only a few hundred nanometers in thickness (or height). An entire foliar sheet may be quite large depending in part on the dimensions of the shell, and is composed of many laths laying side by side. Each lath may be typically about 2 μm wide and perhaps up to 10 μm long (Watabe *et al.*, 1958; Watabe and Wilbur, 1961; Watabe, 1965).

We have suggested that the organic component of folia

consists of foliar globules, which themselves appear to be composites of protein and mineral. The foliar globules are packed closely together and overlay each foliar lath (Sikes *et al.,* 1998). A typical foliar globule is formed into an ellipsoid of about 10 to 40 nm in height, 50 nm in width, and 100 nm in length. Evidence from chemical, enzymatic, immunologic analyses and from both atomic force microscopy (AFM) and scanning electron microscopy (SEM) suggested that the globules are proteinaceous. On the other hand, it also appeared that the foliar globules are mineralized, as evidenced by their dimensions, the measured content of protein in foliar layers, and their invariant appearance when viewed by AFM both dry and in fluids. However, when subjected to conditions of supersaturation with respect to calcite in artificial seawater, including periods of spontaneous nucleation and crystal growth in the bathing fluid, the foliar globules generally did not support crystal growth as viewed continuously by AFM.

The purpose of this investigation was to further probe the identity of the foliar globules through pyrolysis followed by AFM and SEM comparisons of the pyrolyzed and non-pyrolyzed foliar surfaces. Pyrolysis was selected for this purpose because the foliar globules were resistant to treatment with HOCl and NaOH, presumably due to the shielding effect of the mineral component (Sikes *et al.,* 1998). The foliar globules were pyrolyzed by subjecting them to 475°C for 36 h, conditions that are reported to remove all of the organic matter without affecting the mineral (Paine, 1964; Price *et al.,* 1976; Dean, 1992).

Crystal nucleation and growth on pyrolyzed and control surfaces were monitored at supersaturations (Ω) over the range of $\Omega = 10.7$ to 52.5. The extent and morphology of crystal formation were revealed, including the influence of Ω on morphology.

The results showed that the pyrolyzed surface was much more active in promoting crystallization at all levels of Ω. The foliar globules of the control surface did not support crystal formation at the lower values of Ω. At higher Ω, crystals did emerge from foliar globules. These crystals had irregular morphology and appeared to form on the basal (0 0 1) plane of calcite. Conversely, the morphology of ectopic crystals was completely different on pyrolyzed and non-pyrolized (control) surfaces. Morphological and AFM analysis at the atomic level of ectopic crystals on pyrolyzed surfaces suggested that the foliar globules were associated with (1 −1 0) planes and that the *c* axis of calcite was parallel to the long axis of the foliar laths. This indicated that elongation, the principal axis of growth of foliar layers, may occur along the *c* axis, other prominent examples of which include the stacking of nacreous tablets of shells and elongation of echinoderm spicules (Weiner and Addadi, 1997).

The foliar globules did not appear to be nucleation sites for the next foliar layer, at least not at low to moderate levels of supersaturation. Rather, they behaved like composites of protein and (presumably) amorphous $CaCO_3$ that limit thickening of foliar laths and probably contribute to flexibility and durability of the shell. Possible locations for continued mineral growth of the shell include putative, dispersed mineral interconnections along the foliar surfaces, as well as exposed mineral at the leading edges of foliar laths.

A cyclic model of foliar lath formation is proposed on the basis of measured rates of shell enlargement *in vivo,* rates of calcite growth at different levels of Ω *in vitro,* and measured interactions of soluble, oyster-shell protein with calcite *in vitro.* The model includes pulsed secretion for a minute or so of matrix proteins, largely in gelling form, followed by removal of the protein from the mineralizing fluid upon binding to exposed mineral. This interaction of matrix and mineral would limit and shape the underlying mineral lath. Mineral deposition of the next layer would then ensue at relatively high Ω over a time frame of about 1 h. These events would be repeated, with a new foliar layer formed at each turn of the cycle.

Materials and Methods

Oyster shell folia

Freshly shucked shells of the Eastern oyster, *Crassostrea virginica,* were gently fractured by compression with a Carver press at a loading of about 200 psi. Large fractured fragments of shell were then held manually to maintain their orientation, and white, pearlescent foliated chips were picked out by hand while being viewed with a binocular dissecting microscope so that the external (facing the sea) and internal surfaces (facing the mantle) were known. Control chips were then glued, usually with the inner surface up, onto a 12-mm glass disc on a partially air-dried (5 min) 10-μl droplet of commercial polyurethane (Minwax) diluted 3:1 with dichloromethane to promote rapid drying and thin distribution of the polyurethane on the glass. The amount of polyurethane was minimized such that there was enough to provide stable adhesion of the chip to the glass disc during extended viewing in fluids, but without an excess that might wick up onto the upper surface of the chip. The glass disc itself had previously been glued with cyanoacrylate (which was not compatible with viewing in fluids) to an SEM stub for use with an AFM scanner that had been custom-fitted with an SEM stub holder.

There were no clear differences in appearance between inner and outer surfaces of control chips. Only inner surfaces were studied in control treatments. Following AFM viewing, the same chips then were viewed by SEM.

The chips ranged from 1 to 3 mm in linear dimensions and typically weighed less than 1 mg and not more than 3 mg. This made them big enough to manipulate but small enough that they easily fit in the fluid cell of the AFM (volume of about 150 μl) and did not rapidly deplete soluble

lattice ions during the flow-through conditions of crystal growth.

Pyrolysis

About 10 foliar chips were placed in a 30-ml glass vial for each treatment in a muffle oven (Blue M Electric Co.) at 475° ± 10° C for 36 h. Following pyrolysis, some vials were capped and the chips stored in air. Other vials were fitted with gas-tight caps and the vials purged with dry nitrogen. The purpose of this treatment was to control for the possible reaction of CO_2 in humid air with the pyrolyzed surface. In yet other cases, some of the pyrolyzed chips were rinsed three times in the vials with 10 ml of $CaCO_3$-saturated water with magnetic stirring for 10 min, followed by decanting of the fluid after each rinse. After the last rinse, the chips were manually blotted onto filter paper, then placed back in the vial, and stored in dry nitrogen. The rinsing fluid was prepared as the supernatant of a slurry of 1 g of reagent-grade calcite in 100 ml of water, stirred for at least 24 h. The purpose of rinsing was to remove any pyrolytic products that may have remained on the surfaces.

If the chips were simply stored in air after pyrolysis, their surfaces were observed to change at the nanometer level over a period of weeks. Initially, the pyrolyzed surfaces appeared to be relatively featureless and free of the globular morphology, but powdery until rinsed clean during imaging in saturated artificial seawater. After weeks to months, however, some nanoscale crystals would develop on the surfaces, even though the chips were stored "dry" in air. Presumably these were calcite crystals that formed as a result of cycles of relatively drier and more humid conditions in the saturated, hydrated layer on crystal surfaces in humid air. Accordingly, all images reported herein were taken from chips that were stored in nitrogen.

To verify the method and to observe the relative stability of control calcite surfaces, chips of calcite similar in size to the foliar chips were subjected to the pyrolytic treatment, stored in air or in dry nitrogen, and observed by AFM both dry and in fluids. The calcite chips were obtained by gently striking a large calcite rhombohedron (~4 cm in length; Watkins Mineral Corp., Wichita Falls, Texas) with a razor edge, producing small rhombohedral fragments. All surfaces of these rhombohedrons were observed by AFM to be the (1 0 4) cleavage surfaces and remained so after pyrolysis, which is understandable in that calcite is stable up to ~825° C (Boynton, 1980; Dean, 1992), above which calcite decomposes to calcium oxide. Crystallographic details and AFM images of calcite (1 0 4) surfaces are presented in following sections about crystal formation on foliar laths.

There was some surface roughening at the nanometer level of the pyrolyzed surfaces of the control, calcite rhombohedrons, which again might result from heating the saturated, hydrated layer. When placed in calcite-saturated fluid, these surfaces smoothed out in a matter of minutes, forming irregularly bordered steps along (1 0 4). When placed in calcite-supersaturated fluid, accretion along the (1 0 4) steps was easily seen, and no surfaces other than (1 0 4) calcite were observed.

The day prior to viewing by AFM, single foliar chips were removed manually from the vial and glued onto glass discs attached to stubs as described above. The chips were then stored overnight in a plastic box so that the polyurethane adhesive became firm. The box was not completely gas-tight, but it was purged with dry nitrogen, shut, and sealed along the edges with Parafilm. Including this treatment, and the interval of up to an hour while the chip was being aligned and positioned under the AFM probe, the chips were only minimally exposed to the atmosphere.

Atomic force microscopy and the crystal growth assay

Constant-force, contact-mode AFM (Digital Instruments) was used, including a flow-through AFM crystal growth assay, as previously described (Sikes *et al.*, 1998). The artificial seawater of the crystal growth experiments consisted of 0.5 *M* NaCl, 0.01 *M* KCl, 0.01 *M* $CaCl_2$, with $NaHCO_3$ varied over the range of 2 to 10 m*M*. The solutions were prepared at 200 ml in a 250-ml, water-jacketed, glass beaker (Fisher Scientific). Reactions were thermostated at 25° ± 0.1°C by use of a recirculating bath (Neslab, model RTE-210). Fluids were pumped through the fluid cell of the microscope at 75 μl min^{-1} by use of a peristaltic pump (Cole-Parmer, Masterflex) with Silastic tubing.

The pH of the fluids was adjusted to 8.32 ± 0.02 and monitored continuously by pH meter and strip chart. In most experiments, the solutions were completely metastable during the course of crystal growth (*i.e.*, supersaturated but not spontaneously nucleating) such that the pH held steady throughout, both in the inflow and outflow of the fluid cell. This showed that the conditions of crystal growth were essentially held constant, at least in the bulk phase, even when crystals were growing on the surfaces of the folia. This constancy was achieved by keeping the foliar surface area low relative to the volume of the fluid cell and the rate of flow through it. In some cases at higher levels of dissolved inorganic carbon (DIC), crystals of calcite would spontaneously nucleate in the bulk fluid after a few minutes (at 10 m*M* DIC) or about 20 min (at 7 m*M* DIC). In these situations, the pH would drift downwards as carbonate ions were removed from solution.

At least three chips were imaged at each supersaturation, including several separate surfaces per chip, except for the treatments at 8 and 10 m*M* DIC. Under these conditions, crystallization was so rapid and widespread that the suspended crystals interfered with the laser signal of the AFM. In addition, crystals rapidly overgrew each other on the foliar surfaces, obscuring the morphology. In the experiments at lower supersaturations, images were collected at intervals during the period of crystal growth, ranging from

several dozen to as many as 200 images per experiment, with a total of approximately 2000 images examined.

Surfaces that exhibited homogeneous foliar morphology were purposefully selected for study. Chips from fractured oyster shell often exhibited surfaces that were more prismatic, chalky, and amorphous, or had mixed morphologies. When these were encountered, the AFM probe was either moved to another location or, if necessary, the chip was discarded.

Scanning electron microscopy

Foliar chips were dehydrated by vacuum at 1 mTorr for 15 min, then coated with a layer of approximately 35 nm of gold in a Hummer X sputter coater (Anatech, Ltd.). Specimens were viewed with a JEOL 848 scanning electron microscope operated at 35 kV.

Calcite models and morphology of ectopic crystals

Computer models of calcite morphology and atomic patterns of lattice planes were made using Cerius[2] molecular modeling software (version 4.0, Molecular Simulations, Inc., San Diego, CA). Plane angles of ectopic crystals and foliar surfaces were measured by means of cross-sectional analysis of AFM images (raw data, before flattening) using AFM imaging software (version 4.1, Digital Instruments, Santa Barbara, CA). Measurements of vertical angles greater than 55° may be subject to a kind of AFM tip artifact, which registers such angles as being approximately 55°. Although this may have been encountered in some cases in the present studies, it certainly was not always the case, with angles significantly greater than 55° frequently encountered. Details of calibration of AFM scanners for measurements of length, width, height, and atomic spacings, as well as procedures to guard against other possible AFM artifacts are given in Sikes *et al.* (1998).

Calculation of supersaturations

Supersaturations (Ω, Table 1) were obtained for calcite at the various levels of DIC for the artificial seawater by use of Mineql+ (version 3.0, Environmental Research Software, Hallowell, ME). The calculation involved dividing the solubility constant for the synthetic seawater (log Ksp = −7.27) into the product of the concentrations of free, ionic calcium ($\sim 10^{-2}$ *M*) and carbonate (level of DIC multiplied by an ionization fraction for CO_3^{2-}, both corrected for ion pairing).

Table 1

Calculated supersaturations (Ω)[a] of artificial seawater[b] with respect to calcite, as determined by use of Mineql+

Calcium (m*M*)	Free ionic Ca^{2+} (m*M*)[c]	DIC (m*M*)	Free ionic CO_3^{2-} (*M*)[d]	Ω
10	9.91	2	$5.85e^{-5}$	10.7
10	9.82	3	$8.78e^{-5}$	16.3
10	9.78	5	$1.46e^{-4}$	26.9
10	9.70	7	$2.05e^{-4}$	37.2
10	9.66	8	$2.34e^{-4}$	42.7
10	9.57	10	$2.93e^{-4}$	52.5

[a] Calculated as: (free ionic calcium) (free ionic carbonate)/solubility product; representative value for log $K_{sp} = -7.27$ (also based on concentrations of free ions, varies only slightly depending on the ionic composition for each experimental treatment).

[b] 0.5 *M* NaCl, 0.01 *M* KCl, pH 8.30, 25°C, closed to the atmosphere.

[c] Takes ion pairing into account, which increases with increasing DIC.

[d] Takes into account the ionization fraction for carbonate at pH 8.30 as well as ion pairing, particularly as sodium carbonate, in the artificial seawater.

Results

Figure 1 is an atomic force (AF) micrograph of a control chip of fractured oyster shell showing the overall foliar morphology of several sheets of calcite composed of laths lying side by side. A detailed view of a surface of this chip, showing the foliar globules, is shown in the AF micrograph of Figure 2.

The untreated foliar globules in general did not support crystal growth under conditions of $\Omega = 10.7$ or $\Omega = 16.3$ for periods up to 5 h of fluid flow, although crystals did grow in these experiments at edges and scattered sites, where mineral presumably was exposed on the fractured surfaces. The same foliar surface of Figure 2 is seen in Figure 3 after 60 min at $\Omega = 26.9$. Under these conditions, the foliar globules enlarged, and some began to exhibit crystalline morphology, but most retained an amorphous globular morphology (Fig. 4). In general, it was difficult to obtain atomic patterns from the surfaces of the globules as they emerged; however, a hexagonal pattern that was typical of the uppermost surfaces of the emerging globules is shown in Figure 5.

A representative AF micrograph of a foliar chip that was pyrolyzed is shown in Figure 6. Several foliar sheets are evident; again, each is composed of individual laths laying side by side. At this magnification, the control and pyrolyzed chips had similar appearances.

However, as shown in Figure 7 (an unwashed surface, stored in nitrogen, imaged dry), after pyrolysis, the foliar globules were reduced to fragile remnants. These quickly washed away upon viewing in fluid, as seen in Figure 8 (similar surface, stored in nitrogen, but imaged in artificial seawater, saturated with calcite). Although the globules were removed by pyrolysis, after washing the surface was not featureless, but was covered with very small mineral protrusions. When subjected to $\Omega = 10.7$, these protrusions clearly began to grow such that by 5 h, a uniform pattern of obliquely inclined crystal elements was evident (Figs. 9–11). When $\Omega = 16.3$, the crystal elements emerged much more rapidly; by 60 min, they had merged and overgrown

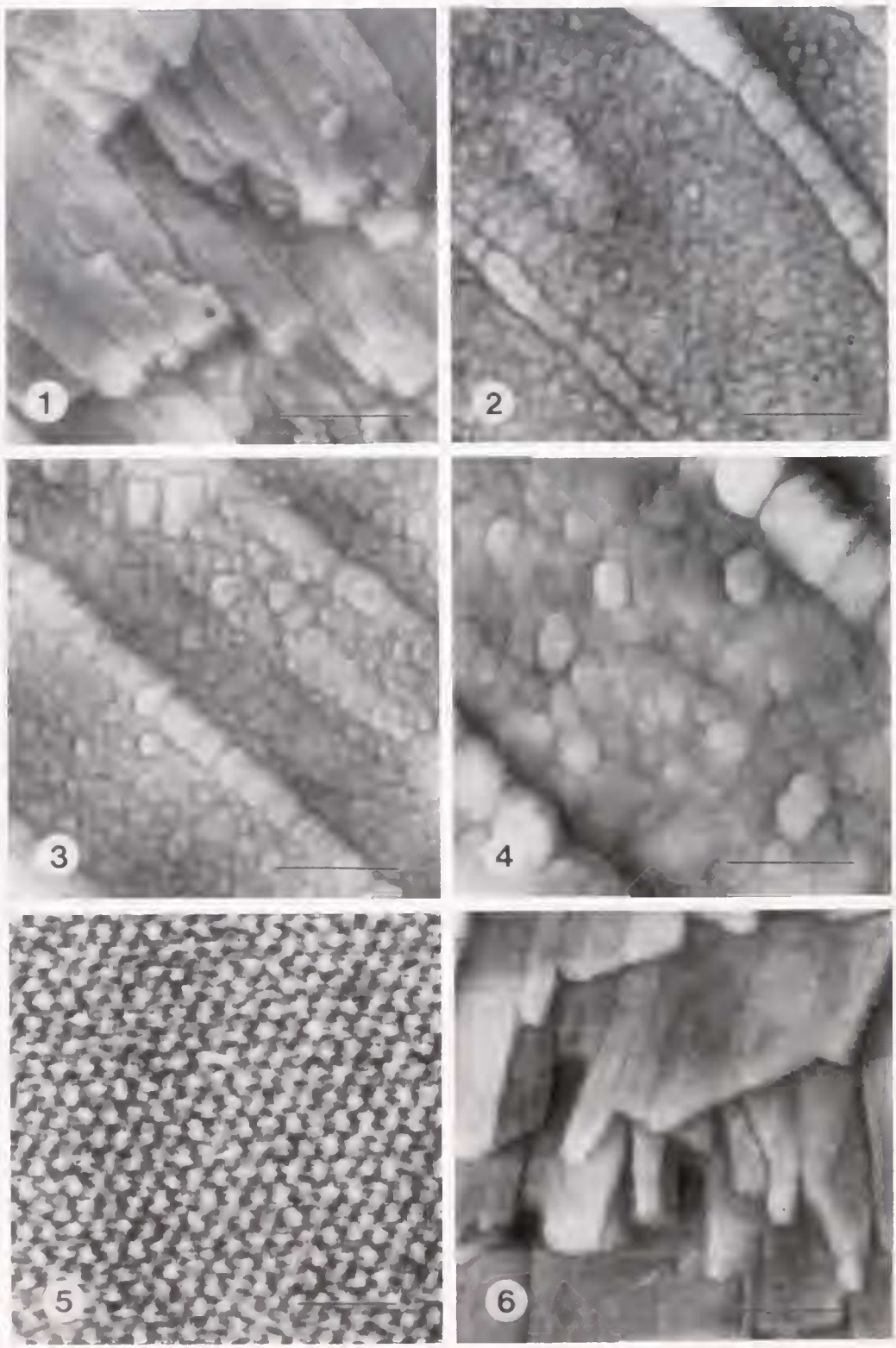

each other, obscuring the original morphology and surface structure (Figs. 12–14).

At $\Omega = 26.9$, crystal growth on pyrolyzed foliar surfaces was essentially instantaneous. Each ectopic crystal had a singular, uniform morphology and orientation along the foliar laths (Figs. 15, 16). For example, as seen in Figure 16, each of the crystals had a shallower surface, that ramped upwards from right to left at an angle of about 45°. The

Figures 1-6. Atomic force micrographs of foliar chips from fractured oyster shell, viewed in artificial seawater.

Figure 1. An untreated, control foliar chip. Total range of elevation within the imaged area = 500 nm; lath heights range from 100 to 260 nm. Scale bar = 2.5 μm.

Figure 2. A foliar surface of the chip of Figure 1. Foliar globular heights range from 10 to 40 nm. The globules are often arranged in linear arrays as shown here, aligned with the long axis of the laths. Scale bar = 0.5 μm.

Figure 3. The foliar surface of Figure 2, viewed in artificial seawater after flow-through crystal growth for 60 min at 10 m*M* calcium, 5 m*M* inorganic carbon, pH = 8.3 (Ω = 26.9; see the text). The foliar globules had emerged somewhat and some began to assume crystalline forms: globular heights range from 15 to 50 nm. Scale bar = 0.5 μm.

Figure 4. The foliar surface of Figure 3, same treatment as in Figure 3, showing details of the emerging foliar globules. Scale bar = 0.25 μm.

Figure 5. The atomic pattern of one of the globular surfaces of Figure 4, imaged by contact-mode AFM in artificial seawater, saturated with respect to calcite. Notice the hexagonal pattern of the atoms, consistent with the theoretical spacing of the (0 0 1) surface of calcite (see the text). Scale bar = 2 nm.

Figure 6. A pyrolyzed foliar chip from fractured oyster shell. Total range of elevation within the imaged area = 400 nm. Lath heights range from 120 to 200 nm. Scale bar = 2.5 μm.

other two surfaces of each crystal emerged from the foliar surface diagonally (from upper left to lower right, and from lower left to upper right) at angles of about 70°, as also seen in the SEM of Figure 17. The smallest such crystals that were seen were about 20 nm in length or width and 3 nm in height. This particular experiment was replicated six times, with the same results and morphology of ectopic crystals each time.

Computer models for the purposes of illustrating the possible orientations of ectopic calcite crystals and the angles of their surfaces relative to the substrate are shown in Figures 18 and 19. The atomic relationships of the crystal lattice are shown in Figure 20.

Generally the upper corner was rapidly completed even in the smallest of the crystals that were grown at Ω = 26.9 (Figs. 15–17), and there were no flat regions to probe. However, in a few cases, it was possible to obtain an atomic pattern from the top surface of a forming corner of such an ectopic crystal (Fig. 21). For comparison, the atomic pattern of the sides of the crystals (Fig. 22) was not difficult to obtain, particularly when the laths were presented at an angle relative to the AFM probe so that the sides of the crystals were close to perpendicular relative to the probe. Computer models that we interpret to correspond to the top surface (Fig. 23) and side surfaces (Fig. 24) are also presented.

Correlations between the computer models and the experimental observations. The model in Figure 19 illustrates the general features of the calcite rhombohedron of six sides and eight corners, shown here truncated with small planar surfaces and with the *c* axis vertical, in the plane of the page. The sides (cleavage planes) are the same crystallographically in terms of the spacings of atoms of calcium and molecules of carbonate; they are referred to as the (1 0 4) family of planes. An atomic pattern of a (1 0 4) surface as observed by AFM is shown in Figure 22, and the corresponding computer model of the protruding oxygen atoms of the (1 0 4) surface is shown in Figure 24.

The corners of the calcite rhombohedron, however, are not all the same. In the model of Figure 19, the top and bottom corners are crystallographically equivalent to each other, here truncated with basal (0 0 1) planes, which are perpendicular to the *c* axis (atomic patterns as in computer model of Fig. 20). A crystal that nucleates from a horizontal (0 0 1) plane would form a three-sided pyramid with the *c* axis perpendicular to the nucleating surface. The upper corner would be perfectly centered at the point where the three planes meet. Each plane would occur at an angle of 22.31° with the nucleating surface, as shown in the model of Figure 18b.

On the other hand, the other six corners of the calcite rhombohedron are also crystallographically equivalent to each other and are formed at points where three cleavage planes meet that are not so symmetrically arranged. If one of these corners is turned uppermost so that the *c* axis is horizontal and (0 0 1) vertical, the horizontal planes would be among the family of planes of which (1 −1 0) is a member (atomic patterns as in the model of Fig. 23). A crystal that nucleates from the (1 −1 0) family of planes would form a three-sided pyramid having two sides that form angles of 69.43° with the nucleating surface, with the third side forming a shallower angle of 44.37°, as shown in the model of Figure 18a, and as observed experimentally in the AFM and SEM images of Figures 15–17.

Discussion

Crystallographic aspects

The foliar globules were reduced by pyrolysis to fragile remnants that were firm enough to be imaged by AFM when dry but were rapidly washed away when imaged in calcite-saturated, artificial seawater. This suggested that the globules lost an organic component on pyrolysis but retained a mineral component that either dissolved, broke apart, or both upon treatment with the fluid. These results are consistent with prior evidence from chemical, enzymatic, im-

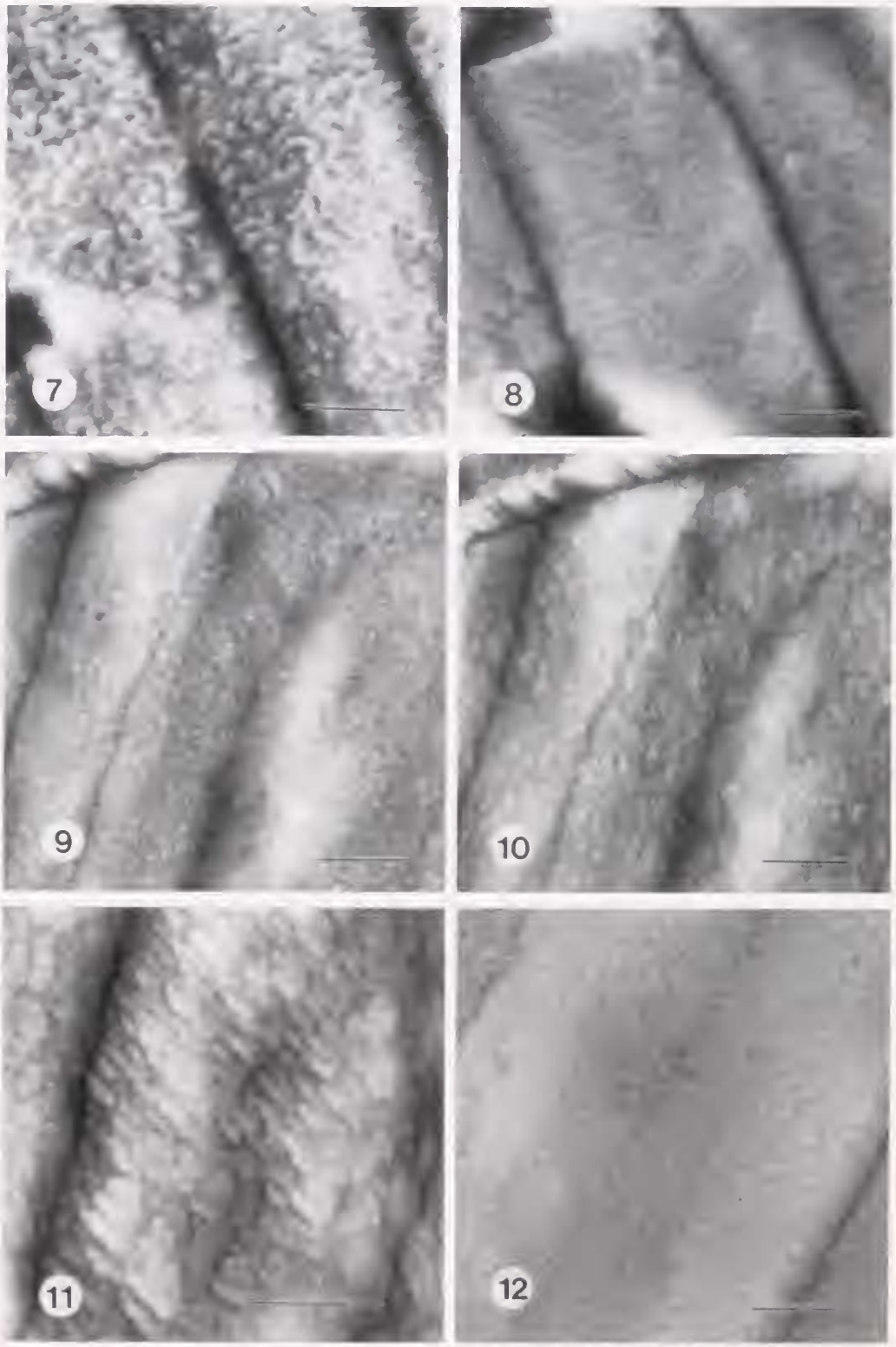

munologic, and morphological approaches that had indicated that the foliar globules appeared to be agglomerations of protein molecules and mineral, presumably amorphous calcium carbonate plus other minor constituents (Sikes *et al.*, 1998).

The foliar globules had no crystallographic surface fea-

Figures 7–12. Atomic force micrographs of pyrolyzed foliar chips from fractured oyster shell.

Figure 7. Chip viewed dry. The chip had not been rinsed after pyrolysis. It was stored in nitrogen in a gas-tight vial. Heights of foliar remnants ranged from 8 to 24 nm. Scale bar = 0.5 μm.

Figure 8. Chip viewed in artificial seawater, saturated with respect to calcite. Foliar globular remnants had mostly dissolved or washed away, revealing a fine crystalline texture of crystal elements with heights of about 2 nm that emerge obliquely from the foliar surface. Scale bar = 0.5 μm.

Figure 9. Chip viewed in artificial seawater after flow-through crystal growth for 10 min at 10 m*M* calcium, 2 m*M* inorganic carbon, pH = 8.3 (Ω = 10.7; see text). The crystal elements of the foliar surface began to become more visible. The lateral emergence of crystal blocks from the edges of laths can be seen at the upper left of the image. Scale bar = 0.5 μm.

Figure 10. The same pyrolyzed foliar surface as in Figure 9, viewed under the same conditions after 5 h of crystal growth. The crystal elements of the foliar surface had clearly enlarged: height of the emerging crystal ranged from 2 to 8 nm. Again, the lateral emergence of crystal blocks from the edges of laths can be seen at the upper left of the image. Scale bar = 0.5μm.

Figure 11. The same pyrolyzed foliar surface as in Figure 10, viewed under the same conditions after 5 h of crystal growth. Details of the emerging crystal elements can be seen, including the oblique angle at which they emerge from the foliar surface. Scale bar = 0.25 μm.

Figure 12. A chip viewed in artificial seawater, saturated with respect to calcite. Some of the texture of the crystal elements of the foliar surface can be seen. Scale bar = 0.5 μm.

tures such as planes or angular aspects, and no atomic patterns were obtained from them by AFM. The term *amorphous* is used here to emphasize this lack of crystalline features; it is not necessarily meant to ascribe an exact equivalence between the mineral of the foliar globules and amorphous $CaCO_3$ that might be formed inorganically at high Ω, although such an equivalence is certainly possible. The probable occurrence of amorphous $CaCO_3$ within carbonate biominerals has long been inferred (Lowenstam and Weiner, 1989; Simkiss and Wilbur, 1989; Simkiss, 1994) and has received increased attention as both a common and abundant component of such structures (Aizenberg *et al.*, 1996; Beniash *et al.*, 1997; Weiner and Addadi, 1997).

Another possible indication of the amorphous nature of the mineral component was that the foliar globules did not nucleate calcite crystals from solutions at low supersaturations. When supersaturations were purposefully raised to force crystallization, crystals slowly emerged from the globules. Upon enlargement of the crystals such that flat upper surfaces and sides could be probed, these crystals were observed to have (0 0 1) top surfaces and (1 0 4) sides, and eventually formed a symmetrical pyramid at the upper corner. Such crystals evidently emerged from the basal plane of calcite in the form depicted by Figure 18b, and ultimately fused to form aggregates.

These crystals are not thought to indicate the crystal structure of the underlying calcite lath. Rather, nucleation from the basal plane is known to be promoted by polyanionic proteins from biominerals (Addadi and Weiner, 1985; Addadi *et al.*, 1987), which are one component of the globules, or this may simply be a favored mode of growth from an organic/amorphous $CaCO_3$ composite.

The pyrolyzed foliar surfaces consisted of tightly packed arrangements of mineral protrusions, each of a width of about 10 nm, that emerged obliquely from the plane of foliation (Figs. 8–10). The mineral protrusions, like the original foliar globules, exhibited no identifiable, crystallographic features or atomic patterns. Although pyrolysis certainly destroyed most of the organic component, it is possible that some of the binding groups, such as carboxylates and phosphates of the polyanionic proteins, were actually imbedded as part of the crystal lattice (Mann *et al.*, 1990; Wierzbicki *et al.*, 1994; Sikes and Wierzbicki, 1995, 1996), and thus may remain there even when the rest of the protein is gone. Conceivably, this could disrupt the atomic patterns that might otherwise be revealed by AFM.

Even at the lowest supersaturation (Ω = 10.7) of the study, crystals slowly emerged from the pyrolyzed foliar surfaces over a period of 5 h. The general morphology of the underlying, nanoscale crystal elements of the folia was maintained during this interval at this level of Ω. Although no obvious crystallographic features were seen, the crystal elements did appear to emerge with identical orientation at an approximate angle of 45° to the pyrolyzed foliar surface (Fig. 11).

As the supersaturation was increased to Ω = 26.9, however, clearly observable crystallization was almost instantaneous (Figs. 15–17). The crystals, even the smallest ones with nanometer dimensions on the order of crystal nuclei, all had the same morphology and orientation along the foliar laths. In some cases, the uppermost plane, parallel to the plane of foliation, was resolvable at the atomic level by AFM as the (1 −1 0) surface of calcite (Fig. 21). The crystal morphology, including measurements of angles of the sides of the crystals (one side at ~45°, the other two sides of the pyramids at ~70°) relative to the surface, was consistent with calcite nucleating from one of the (1 −1 0) family of planes, with one of the six "nonbasal" corners uppermost, as depicted in Figure 18a. In this morphology, the *c* axis was parallel to the plane of foliation, aligned with the long axis of foliation. Similarly, the foliar globules are frequently so aligned, forming linear arrays along the long axis of foliation (Figs. 2, 3).

Evidently, pyrolysis had removed the foliar globules and

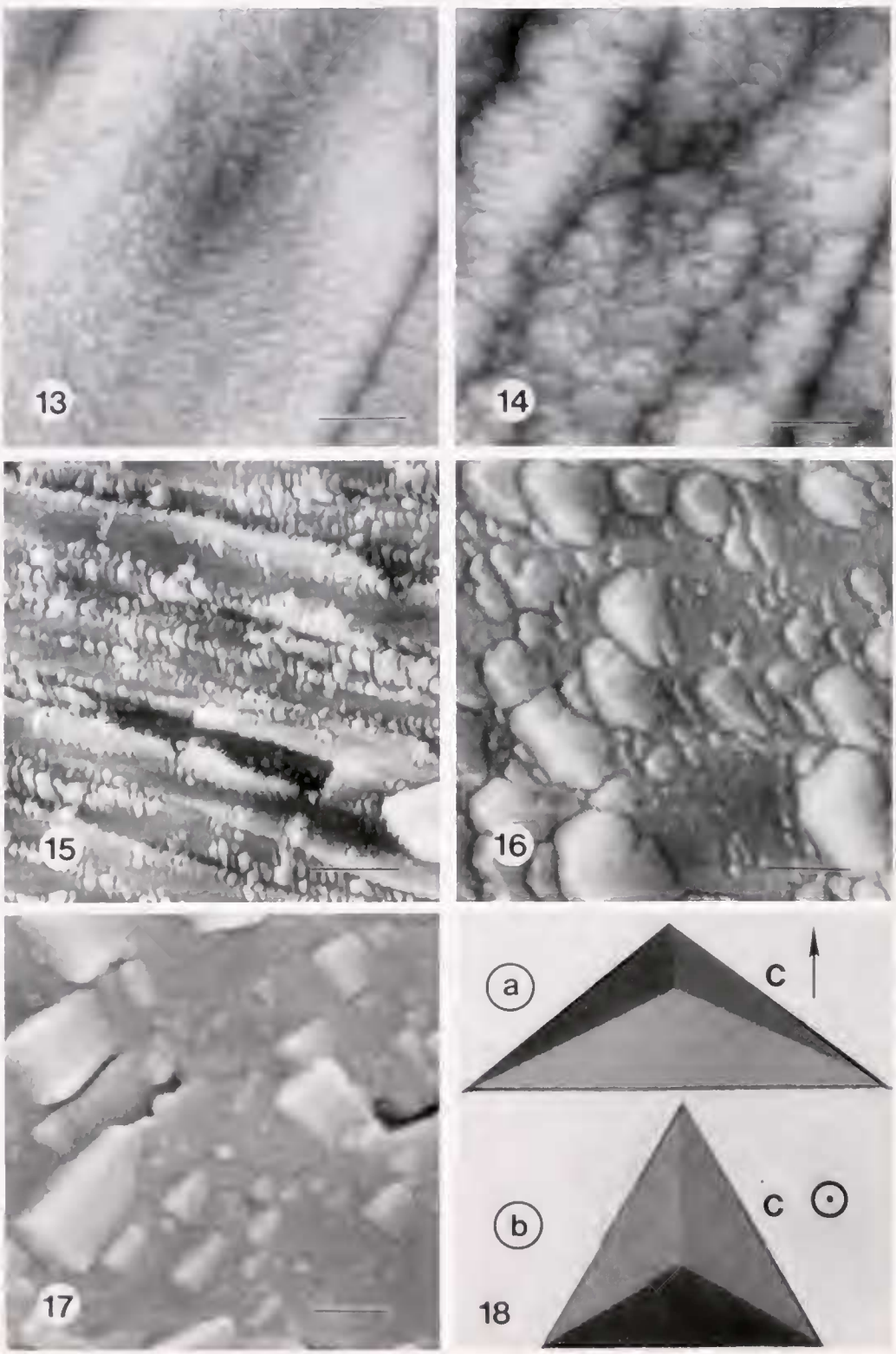

exposed (1 −1 0) surfaces that served as nucleation sites for the ectopic crystals. The soluble proteins from oyster shell, as well as other polyanionic adsorbates, are thought to have high affinity for the (1 −1 0) surface of calcite (Berman *et al.*, 1988; Didymus *et al.*, 1993; Albeck *et al.*, 1996), with binding parallel to the *c* axis being one preferred orientation (Wierzbicki *et al.*, 1994). Therefore, it seems consistent that the foliar globules, to the extent that at some point they have

Figure 13. Atomic force (AF) micrograph of the same pyrolyzed surface as in Figure 12, viewed in artificial seawater after flow-through crystal growth for 6 min at 10 m*M* calcium, 3 m*M* inorganic carbon, pH = 8.3 (Ω = 16.3; see the text). The crystal elements of the foliar surface had enlarged. Scale bar = 0.5 μm.

Figure 14. AF micrograph of the same pyrolyzed surface as in Figure 13, viewed under the same conditions, after 30 min of crystal growth. The crystal elements of the foliar surface had continued to grow, merging into larger forms, overgrowing each other and obscuring the original morphology. Scale bar = 0.5 μm.

Figure 15. AF micrograph of a pyrolyzed foliar chip from fractured oyster shell, viewed in artificial seawater after flow-through crystal growth for 7 min at 10 m*M* calcium, 5 m*M* inorganic carbon, pH = 8.3 (Ω = 26.9; see the text). Large numbers of ectopic crystals of characteristic and uniform morphology and orientation had formed almost instantly on the surface. Height of the ectopic crystals ranged from a few nanometers to 250 nm after 7 min. Scale bar = 2.5 μm.

Figure 16. AF micrograph of the same pyrolyzed surface as in Figure 15, viewed under the same conditions after 10 min of crystal growth. The ectopic crystals had nucleated from the foliar surface as asymmetric, three-sided pyramidal forms, each with identical morphology and orientation. The crystals were essentially everywhere on the surface, with the smallest ones a few nanometers in height, and the largest ones in the imaged area about 200 nm in height. Scale bar = 0.5 μm.

Figure 17. A scanning electron micrograph of a pyrolyzed foliar surface treated the same as in Figure 15, again showing the ectopic crystals that emerged from the foliar surface as asymmetric, three-sided pyramidal forms, confirming the morphology as seen in the AFM images. Scale bar = 0.5 μm.

Figure 18. Computer models of three-sided, pyramidal, ectopic crystals, viewed from above. (a) A crystal that would be nucleated from the (1 −1 0) surface of calcite, with the orientation of the *c* axis shown by the arrow pointing upwards in the plane of the page. The surface of each side would be equivalent and of the (1 0 4) type, but the corner is formed asymmetrically at the point where the three sides meet, such that two sides would emerge from the surface at an angle of 69.43°, with the third side emerging at an angle of 44.37°. This model is consistent with the morphology of the ectopic crystals that were grown on the pyrolyzed foliar surface. (b) A crystal that would be nucleated from the (0 0 1) surface of calcite, with the orientation of the *c* axis shown by the symbol indicating perpendicularity to the page. Each surface would be equivalent to the others, with the corner formed symmetrically at the point where the three sides meet. Each side would emerge from the surface at an angle of 22.31°.

similar polyanionic proteins available for binding to shell calcite, might bind to the (1 −1 0) surface, parallel to the *c* axis.

As suggested by previous workers, it seems reasonable to assume that the ectopic crystals will track the underlying biomineral calcite lattice (Okazaki and Inouyé, 1976; Okazaki *et al.*, 1981; Runnegar, 1984), especially if any organic covering is removed from the biomineral. Following this assumption, the foliar surface would appear to be the (1 −1 0) surface of calcite. In addition, the laths evidently elongate along the *c* axis.

This interpretation is consistent with the X-ray data of Taylor *et al.* (1969), who reported that the plane of foliation was parallel to the *c* axis. These authors noted an inclination of the folia relative to the shell surface and were able to arrange the actual plane of foliation to be parallel to the slide on which the shell was mounted by correcting for an angle of 26° at which the folia emerged to form the surface of the shell. On the other hand, mounting the shell itself as parallel to the slide in effect would rotate the plane of foliation by about 26°, which brings one of the (1 0 4) family of planes as perpendicular to the X-ray beam. This is consistent with the findings of Runnegar (1984), who reported (1 0 4) reflections as indicative of inner surfaces in X-ray work with fragments cut from shell. In addition, Runnegar (1984), following the method of Okazaki and Inoué (1976), also grew ectopic calcite at very high Ω (>1000) on bleached shell surfaces, revealing asymmetrical, three-sided pyramidal crystals, perhaps the same as observed herein.

Other workers (Wada, 1963, 1968; Watabe, 1965, 1981) had observed crystallites on folia that were arranged with the *c* axis vertical to the plane of foliation and therefore thought to be nucleated from the (0 0 1) plane. We have also sometimes seen this on control, foliar chips that have prominent ectopic, polygonal crystals that appeared to be nucleated from the basal plane (not shown). As reported herein, the control foliar surfaces may act as nucleation sites for such basal calcite crystals at relatively high levels of supersaturation.

The cycle of mineralization in vivo

The formation of shells as layers of mineral interspersed with organic sheets implies a cyclic process of organic secretion and inorganic mineral growth (*e.g.*, Degens, 1976; Wheeler and Sikes, 1989). Details central to this process are poorly known but include the *in vivo* levels of Ω and the organic components, as well as the relative timing of secretion of lattice ions and organic matrix. The AFM measurements of growth of calcite on shell fragments, together with measurements of shell growth *in vivo*, may provide a way to estimate the effective Ω *in vivo*, as well as the time frame of lath formation, as explained below.

Starting with the possible levels of lattice ions and organic matrix *in vivo*, measurements of the ionic and organic

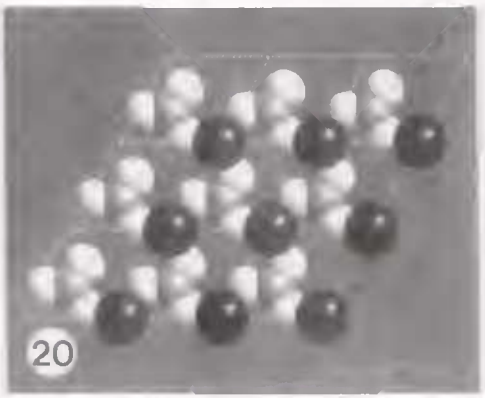

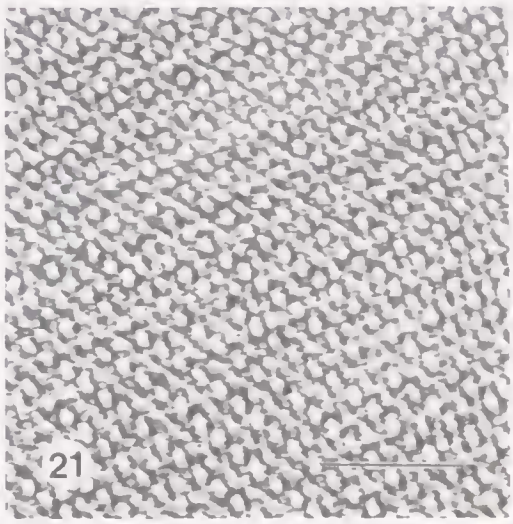

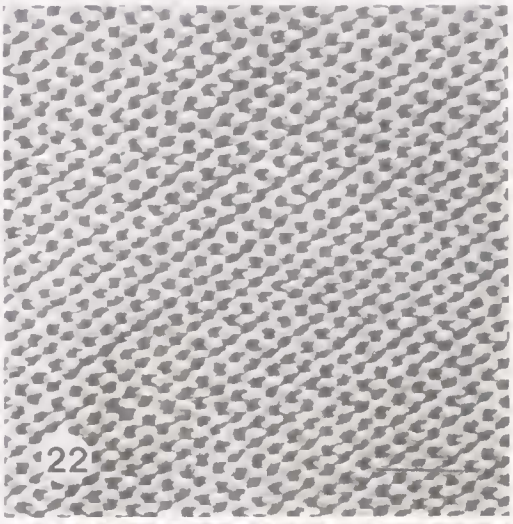

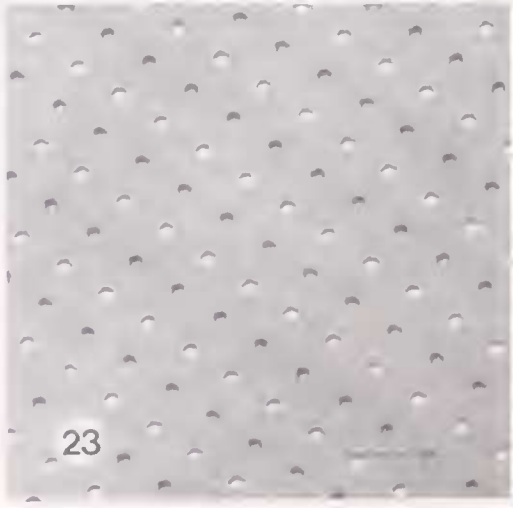

composition of extrapallial fluid (EPF, the medium of shell formation), are available by means of exacting microanalysis following attempts to sample the fluid. In the Eastern oyster, the estimate (Crenshaw, 1972) of calcium content was close to that of seawater at nearly 10 m*M*, inorganic carbon was as high as 5 m*M* (with seawater normally at about 2.2 m*M*), but the pH at about 7.4 was notably lower than typical values for seawater (~8.2), which in turn would result in significantly lower levels of carbonate ion. These conditions of the EPF would convert to an Ω of 2.83, which is quite low. Studies of the EPF of other molluscs yielded roughly similar results (Wada and Fujinuki, 1976; Misiogianes and Chasteen, 1979; Nair and Robinson, 1998).

Moreover, other solutes of the EPF such as magnesium,

Figure 19. Computer model of a calcite rhombohedron. The model is depicted with the *c* axis upward, in the plane of the page. Planes are cut through the eight corners. The arrows indicate the bottom and top planes (basal planes), which are (0 0 1) surfaces. The planes through the other corners are the family of (1 −1 0) planes. Each of the sides is a member of the (1 0 4) family of planes.

Figure 20. A computer diagram of the (0 0 1) surface of calcite, showing an upper plane of calcium atoms, and an underlying plane of carbonate groups. Notice how the calcium atoms coordinate with three oxygens of separate underlying carbonate groups. Each calcium atom also would coordinate with three oxygens of separate carbonate groups of a carbonate homoplane (not shown) that would overlay the calcium plane in a similar manner, with successive homoplanes of calcium and carbonate alternating to form the calcite crystal. The *c* axis runs perpendicular to the (0 0 1) plane. The *a* axes are shown as the grid of lines on the diagram. The (1 −1 0) family of planes also run perpendicular to the (0 0 1) plane (or parallel to the *c* axis), emerging perpendicularly from the *a* axes. Scale bar = 0.5 nm.

Figure 21. Atomic force (AF) micrograph of the atomic pattern of one of the uppermost surfaces of the crystals of Figure 16. The spacings of atoms are consistent with the (1 −1 0) surface of calcite. The more clearly resolved rows of atoms (from upper left to lower right) are thought to correspond to protruding oxygens of carbonate groups, with the atoms that tend to blend together in the other rows (also from upper left to lower right) corresponding to calcium atoms that are somewhat recessed into the surface. Scale bar = 3 nm.

Figure 22. AF micrograph of the atomic pattern of one of the sides of the ectopic crystals as in Figure 16, viewed in artificial seawater saturated with respect to calcite. The spacings of atoms are consistent with the (1 0 4) surface of calcite. In this image, each lattice position is thought to correspond to a protruding oxygen atom of the carbonate groups, which are elevated to some extent relative to calcium atoms that occur just below the (1 0 4) surface. Scale bar = 2.0 nm.

Figure 23. A computer diagram of the (1 −1 0) surface of calcite, showing the oxygen atoms (white) of the carbonate groups outermost and the calcium atoms (gray) slightly recessed into the surface. The number of oxygen atoms per unit area of this surface is not nearly as dense as in the (1 0 4) surface, and therefore both the oxygens and the calcium atoms can be seen in AF micrographs of the (1 −1 0) surface. The atoms within one row of oxygens are spaced 4.99 Å apart, with the nearest oxygens in separate rows 8.53 Å apart. This matches within 5% of the atomic spacings of the uppermost, forming surface at the corner of one of the ectopic crystals on a pyrolyzed foliar surface as seen in Figure 21. Note that if only every other row of oxygens of the (1 0 4) surface has the atoms clearly resolved, with the other rows of oxygens having atoms blurred together (again with no calcium atoms observed at all), which can be done by increasing the force of the AFM probe as well as the gain setting, a pattern somewhat similar to the (1 −1 0) pattern can occur. However, the spacings and angles between atoms of the two surfaces still differ, as does the number of atoms per unit area. Scale bar = 1.0 nm.

Figure 24. A computer diagram of the (1 0 4) surface of calcite, showing only the outermost oxygen atoms of carbonate groups, as are seen in AF micrographs of this surface. The calcium atoms are recessed by about 1 Å into the surface and do not show up in AFM's due to the closeness of the surface oxygen atoms. The nearest neighbors of outermost oxygen atoms form rhombohedrons with spacings of 4.24 and 4.99 Å, which matches within 5% of the spacings as seen in Figure 22 of the sides of the ectopic crystals on a pyrolyzed foliar surface. Scale bar = 2.0 nm.

phosphate, small chelants that bind soluble calcium, and organic components like soluble shell proteins are all inhibitory to calcite formation. If these constituents are taken into account, the measurements actually suggest that the EPF is undersaturated with respect to calcium carbonate.

In this regard, Wilbur and Bernhardt (1984) attempted an *in vitro* assay for calcite formation based on prior estimates of the content of EPF. It was necessary to raise calcium to 28.2 m*M* and inorganic carbon to 7.6 m*M* at pH = 8.33 (including Mg at 47.2 m*M*, but no phosphate and no organic compounds) to obtain nucleation after about 20 min at 21°C. These levels of soluble lattice ions correspond to Ω = 72.4. In the absence of Mg, under otherwise similar conditions, we obtained nucleation after about 20 min at Ω = 37.2.

By comparison, seawater itself is considered to be mildly supersaturated with respect to calcite ($\Omega \sim 10$). However, again, the other constituents such as magnesium, phosphate, and organic components act to stabilize seawater so that calcium carbonate does not normally precipitate.

Turning to rates of shell deposition *in vivo*, on the other hand, direct measurements of shell enlargement revealed substantial rates of carbonate deposition that are indicative of notably high supersaturations. For example, in the scallop *Argopecten irradians* and the marine clam *Mercenaria mercenaria*, shell enlargement was measured by radioisotopic approaches to range from about 0.1 to 2.0 μm cm^{-2} h^{-1} (Wilbur and Jodrey, 1952; Wheeler *et al.*, 1975; Wheeler and Wilbur, 1977; Dillaman and Ford, 1982). By dividing by the density of shell, this value was converted to an increase of a single linear dimension such as thickness or elongation of about 35 to 700 nm cm^{-2} h^{-1}.

Regarding the possible levels of Ω *in vivo* as indicated by AFM observations of calcite growth *in vitro*, the measurements of calcite formation on pyrolyzed foliar surfaces under controlled conditions of supersaturation indicated an

emergence of foliar crystal elements of about 1 to 2 nm h^{-1} at $\Omega = 10.7$. At $\Omega = 16.3$, the average crystal growth over the surface was about 100 to 150 nm h^{-1}. At $\Omega = 26.9$, on average, the ectopic crystals emerged from pyrolyzed foliar surfaces at 300 to 500 nm h^{-1}. Comparison of these values to the above-referenced measurements of shell thickening suggests that the levels of Ω locally within the EPF must have been in the range of about 16 to 27, and perhaps even somewhat higher, exclusive of the effects of any inhibitory constituents of the EPF that may have been present. If soluble inhibitors of calcite formation were present, the levels of Ω would need to be even higher to drive the observed rates of shell growth.

One issue that affects direct measurement of constituents of the oyster EPF is the ability to obtain fluid for analysis. The mantle lies essentially in contact with the shell and the volume of EPF available for sampling is thus minimal to nonexistent (*e.g.;* see figure 9 of Watabe, 1974; figure 1 of Erben and Watabe, 1974; and figures 2 and 4 of Bevelander and Nakahara, 1980). Consequently, direct analysis of the actual levels of lattice ions and various inhibitors or promoters of crystallization in the fluid of mineralization may be impossible (Wheeler and Sikes, 1989; Wada, 1990)—assuming that there is a fluid as such. Having some bearing on the question of whether fluid is present is Galtsoff's view (1964) that mineralization in the oyster is a kind of solidification within a gel-like layer that is deposited by the mantle on the shell as it grows. He observed rhythmic back-and-forth movements by the mantle on the shell along the direction of foliation. These movements were accompanied by deposition of a highly viscous coating, which subsequently became mineralized (see also Carriker *et al.*, 1980; Carriker, 1996). Crenshaw (1990) and Calvert and Crockett (1997) have further reviewed aspects of biomineral formation within a possibly gel-like precursor.

When extracted by slow dissolution of shell, the shell matrix proteins, most of which are fundamentally similar in amino acid composition, are collected over a continuum of molecular weights (M_w) that ranges into the millions and higher (Wheeler *et al.*, 1988). The higher M_w fractions are gelling materials that are highly interactive with water but not actually water-soluble (Wheeler and Koskan, 1993; Wheeler *et al.*, unpubl. obs.). Some of the lower M_w materials that are released from shell as soluble fractions might also be linked to the gelling matrix when in the shell, but this is not known.

The possible significance of soluble *versus* gelling proteins bears on the question of the effective supersaturation of the mineralizing environment. Even low doses of soluble protein from oyster shell are strongly inhibitory to calcite nucleation (0.1 μg protein ml^{-1} at $\Omega = 42.7$; Wheeler and Sikes, 1989) or growth of calcite seed crystals (0.015 μg protein ml^{-1} cm^{-2} at $\Omega < 5$; Low, 1990; Wheeler *et al.*, 1991). The incorporation of the soluble protein into the crystals under these conditions was measured at 0.4 to 0.5 μg μmole $^{-1}$ calcite (Sikes and Wheeler, 1986), which is approximately equal to the amount of the protein that occurs in the folia.

However, if the shell is to grow at the rates that have been measured *in vivo*, which would require levels of Ω that are significantly elevated relative to seawater, it would seem that the shell protein, if present at all during intervals of mineral deposition, would occur in the mineralization fluid in soluble form at levels too low to account for the amount of protein in shell. However, this problem could be overcome if the secretion of shell protein by the mantle were episodic such that intervals of shell growth, during which no inhibitory proteins were present at the site of crystallization, were followed by intervals during which the newly formed mineral layer became covered by proteinaceous material.

In this framework, the measurements of inhibition of calcite formation *in vitro* at low doses of samples of whole EPF (Wilbur and Bernhardt, 1984) may be understood. When 210 μl of EPF from *M. mercenaria* was added to a calcite growth assay, inhibition was observed at roughly the level of 0.1 μg protein ml^{-1} established in other studies (Wheeler and Sikes, 1989). Given the volumes used in the assay, this would suggest that the EPF sample contained about 3 μg of protein, or roughly 15 μg protein ml^{-1} of EPF. This is such a high level that it would totally inhibit shell growth, even at very high Ω, if the protein molecules were present in a soluble form that could interact with the crystal surfaces. On the other hand, if a pulse of protein into the EPF was layered quickly onto a fresh mineral layer of shell and followed by an interval of protein-free EPF of Ω in the range of 16 to 27, the pattern of mineral deposition that is observed in foliar layers could occur. If such intervals of pulsed secretion are on the order of minutes, then samples of EPF, which consist of pooled volumes collected over periods of hours (Wada, 1990), would always contain shell proteins. There is evidence to support these speculations, as follows.

First, the foliar laths have thicknesses in the range 100 to 350 nm. As cited above, the shells of various molluscs have been measured to thicken at rates of 100 to 700 nm h^{-1}, thus formation of individual laths appears to occur at a rate of about 1 or more per h. Each lath is covered by a layer of foliar globules, which are thought to consist of shell protein and amorphous $CaCO_3$. This morphology is consistent with pulsed secretion of the protein, perhaps during an interval of only a few minutes per hour, when the protein is removed from solution by binding to the previously formed mineral. Following that, a period on the order of an hour of protein-free crystal growth would occur. Next, a new organic layer, which appears initially to be a gel (Wheeler *et al.*, unpubl. obs.), is secreted, binds to the lath, and subsequently becomes covered by calcite. Thus, the gelled organic layer also becomes mineralized during this process, apparently in the form of amorphous $CaCO_3$ of the foliar globules.

Conceivably, the next layer of calcite could nucleate from

the organic layer, from exposed areas of calcite of the underlying lath, or both. That there are exposed areas of calcite even after the organic layer is bound seems probable because the pyrolyzed foliar chips were firm and did not crumble on handling following removal of the organic materials. This suggested that the mineral was continuous throughout the layers of folia. Direct evidence of continuity of this type has been observed between aragonitic tablets of the nacreous layers of shells (Watabe, 1981; Giles *et al.*, 1995). If there are areas of exposed calcite on the foliar surfaces after the organic layer is bound, these would serve as ready nucleation sites for new laths. Such exposed areas of calcite were not visually evident in the AF micrographs of fractured surfaces of folia, and therefore would necessarily be very small, presumably on the scale of nanometers.

The foliar globules themselves were not particularly effective as nucleation sites, and calcite crystals that were nucleated from them by raising the level of Ω did not appear to have the crystallographic orientation and morphology of the pyrolyzed lath. Hence, each succeeding foliar layer seemed to track the mineral of the underlying layer rather than to derive from the amorphous character of the foliar globules.

Another line of evidence that is consistent with the notion of a cycle of mineralization as presented above involves measurements of interactions of the soluble protein from oyster shell with calcite *in vitro*. When the protein was bound to calcite crystals, the maximum capacity of binding was 0.18 μg cm^2 (Wheeler *et al.*, 1991). Taking a value of 0.5% protein by weight in foliar shell, which agrees well with measurements of protein content of shell extracts, including foliar layers (reviewed in Sikes *et al.*, 1998), and with radioisotopic incorporation of the protein into calcite *in vitro* (Sikes and Wheeler, 1986), there would be 0.5 μg protein per μmole (100 μg) calcite. Using 2.6 as a typical value for the density of shell (Wheeler *et al.*, 1975), there would be 13 mg protein cm^{-3} of shell. If this protein were deployed in layers at 0.18 μg protein cm^{-2}, there would be enough protein to form a stack of 72,222 layers of 1 cm^2 in each cm^3. This corresponds to about 140 nm per layer (including the protein), which is at the low end of the range of thicknesses of a foliar lath.

One problem with these conjectures about binding and coverage involves drawing inferences from *in vitro* studies and applying them to *in vivo* processes. For example, the binding studies were based on measurements of the interaction of the protein with (1 0 4) surfaces of calcite. Moreover, the incorporation studies permitted the protein to interact freely with the growing crystal and likely involved several surfaces. The *in vivo* interaction, on the other hand, appeared mainly to be with the (1 −1 0) surface.

The binding affinity of the protein to the (1 −1 0) surface has been calculated to be higher than to the (1 0 4) surfaces (Wierzbicki *et al.*, 1994; Sikes and Wierzbicki, 1995, 1996). However, the binding capacity and coverage of the surfaces would probably be similar. That is, taking the average oyster shell protein as a globule at 50 kD with a linear dimension of about 5.4 nm (Sikes *et al.*, 1998), each unit of protein would cover about 30 nm^2. The maximum capacity of 0.18 μg of protein per cm^2 of calcite would represent 2.17×10^{12} molecules (50 kD = 8.3×10^{-20} g), or a coverage of 6.5×10^{13} nm^2. Comparing this to 1×10^{14} nm^2 per cm^2 suggests that 0.18 μg of the protein would cover most of 1 cm^2 of calcite regardless of the specific surface. Of course, it is also possible that the protein molecules (and the foliar globules) can form more than a monolayer on the calcite of the laths. This in turn would translate into laths of greater thickness as calculated above, which is often seen in the AFM and SEM images, both herein and in prior studies.

Conclusions

Overall, the evidence can be interpreted to support a hypothesis of pulsed secretion of the shell proteins, depletion of the soluble protein from the EPF upon binding to the mineral of laths, and subsequent intervals of growth of new mineral at relatively high Ω. The pulses of shell proteins might occur in a time frame of minutes, with the interval of mineral growth more on the order of an hour. The hypothesis would include secretion of the proteinaceous material primarily as a gelatinous covering that terminates the growth of the underlying lath and defines its surface as a member of the calcite (1 −1 0) family of planes.

In view of the need to elevate Ω to support the observed rates of folia formation *in vivo*, as well as to overcome the influence of soluble inhibitors in the EPF, it seems necessary for the organism to make significant metabolic investment in mechanisms to generate the mineralizing microenvironment. As indicated in many prior studies and reviews, although perhaps not at the magnitude suggested herein, the necessary supply of lattice ions may be provided by mechanisms such as direct active transport of inorganic carbon or calcium, or a combination of transport processes.

Another factor to consider is the formation of the crystals in thin, unstirred layers that are diffusion-limited. Watabe and coworkers (Watabe *et al.*, 1958; Watabe and Wilbur, 1961) noted that folia formation produced tablet-like morphologies that were similar to $CaCO_3$ crystals grown *in vitro* in unstirred layers, probably initiated in an area of highest Ω with growth toward regions of lower Ω, thus producing directional laths. Although crystallization assays often involve high rates of stirring to eliminate diffusion as a rate-limiting variable, some assays have been run under diffusion-limited conditions with concentration gradients into unstirred layers. It is interesting to note that calcium carbonates so produced frequently do exhibit tabular morphologies that resemble foliar laths to some extent, including crystals grown in the presence of shell protein (Fallini *et al.*, 1996; Weiner and Addadi, 1997). In related observa-

tions, Gower (Gower and Tirrell, 1998; Gower, pers. comm.) has noted that at higher concentrations under specific conditions of unstirred supersaturation, low M_w soluble polyaspartates and acidic polypeptides can induce localized droplets of a liquid-like, mineral-precursor phase that converts to calcitic tablets and other $CaCO_3$ structures.

It thus may also be useful to keep in mind that not only can the shell matrix proteins be arranged as the supramolecular assemblage of the gelling material, but also even the soluble molecules of relatively low M_w can agglomerate both in solution and when binding to mineral in the form of ellipsoids of linear dimensions up to about 100 nm (Wierzbicki *et al.*, 1994; Sikes *et al.*, 1998). Such associative behavior of other biomineral proteins such as dentin phosphophoryn, as well as other polyanionic proteins such as casein, has been reviewed by Marsh (1989a, b), who also observed agglomerations of phosphoproteins and mineral salts including amorphous calcium phosphate in nonmineralizing compartments of some molluscs (Marsh and Sass, 1983, 1984, 1985). None of these protein-mineral agglomerations appeared to be very effective as nucleators of crystals of shell or teeth (Marsh, 1986, 1989a, b, 1994).

Similarly, the amelogenins, the principal proteins of the formative stage of tooth enamel, have been shown to form gels composed of agglomerative "nanospheres." These nanospheres have been observed *in vivo* with dimensions of 15 to 20 nm (Fincham *et al.*, 1994, 1995) and *in vitro* with dimensions that range to 100 nm and higher (Wen *et al.*, 1999). The amelogenins are mainly hydrophobic, but they do have anionic C-termini that appear to occur at the surface of the nanospheres and interact there with the calcium hydroxyapatite of enamel. The amelogenin nanospheres are thought to function less in apatite nucleation than in localizing and orienting the developing enamel crystallites prior to their maturation (Fincham *et al.*, 1999).

Examination, by AFM, of the role of such factors and mechanisms in shell formation will require study of calcite growth in the presence and absence of soluble and gelling fractions of oyster shell protein under conditions of static fluids pulsed at different levels of Ω. In addition to further work with fracture surfaces of folia, observations of crystallization on native surfaces of the leading edge where shell formation is initiated will be helpful.

Acknowledgments

This work was supported by grants EHR-9108761 from the National Science Foundation, C-3662 from the Research Corporation, and R/MX-6 from the South Carolina Sea Grant Consortium. We thank JoAn S. Hudson, Director of the EM Facility at [illegible], for her assistance with SEM.

Literature Cited

Addadi, L., and S. Weiner. 1985. [illegible] between acidic proteins and crystals: stereochemical [illegible] in biomineralization. *Proc. Natl. Acad. Sci. USA* **82:** 4110–[illegible].

Addadi, L., J. Moradian, E. Shay, N. G. Maroudas, and S. Weiner. 1987. A chemical model for the cooperation of sulfates and carboxylates in calcite crystal nucleation. Relevance to biomineralization. *Proc. Natl. Acad. Sci. USA* **84:** 2732–2736.

Aizenberg, J., G. Lambert, L. Addadi, and S. Weiner. 1996. Stabilization of amorphous calcium carbonate by specialized macromolecules in biological and synthetic precipitates. *Adv. Mater.* **8:** 222–226.

Albeck, S., S. Weiner, and L. Addadi. 1996. Polysaccharides of intracrystalline glycoproteins modulate calcite crystal growth *in vitro*. *Chem. Eur. J.* **2:** 278–284.

Beniash, E., J. Aizenberg, L. Addadi, and S. Weiner. 1997. Amorphous calcium carbonate transforms into calcite during sea urchin larval spicule growth. *Proc. R. Soc. Lond. B* **264:** 461–465.

Berman, A., L. Addadi, and S. Weiner. 1988. Interactions of sea-urchin skeleton macromolecules with growing calcite crystals—a study of intracrystalline proteins. *Nature* **331:** 546–548.

Bevelander, G., and H. Nakahara. 1980. Compartment and envelope formation in the process of biological mineralization. Pp. 19–27 in *The Mechanisms of Biomineralization in Animals and Plants*, M. Omori and N. Watabe, eds. Tokai University Press, Tokyo.

Boynton, R. S. 1980. *Chemistry and Technology of Lime and Limestone*. J. Wiley, New York.

Calvert, P., and R. Crockett. 1997. Chemical solid free-form fabrication: making shapes without molds. *Chem. Mater.* **9:** 650–663.

Carriker, M. R. 1996. The shell and ligament. Pp. 75–168 in *The Eastern Oyster*, V. S. Kennedy, R. I. E. Newell, and A. F. Eble, eds. Maryland Sea Grant College Publication, College Park.

Carriker, M. R., and R. E. Palmer. 1979. Ultrastructural morphogenesis of prodissoconch and early dissoconch valves of the oyster *Crassostrea virginica*. *Proc. Natl. Shellfish. Assoc.* **69:** 103–128.

Carriker, M. R., R. E. Palmer, and R. S. Prezant. 1980. Functional ultramorphology of the dissoconch valves of the oyster *Crassostrea virginica*. *Proc. Natl. Shellfish. Assoc.* **70:** 139–183.

Crenshaw, M. A. 1972. The inorganic composition of molluscan extrapallial fluid. *Biol. Bull.* **143:** 506–512.

Crenshaw, M. A. 1990. Biomineralization mechanisms. Pp. 1–9 in *Skeletal Biomineralization: Patterns, Processes, and Evolutionary Trends. Volume I*, J. G. Carter, ed. Van Nostrand Reinhold, New York.

Dean, J. A. 1992. *Lange's Handbook of Chemistry*. McGraw-Hill, New York.

Degens, E. T. 1976. *Molecular Mechanisms on Carbonate, Phosphate, and Silica Deposition in the Living Cell*. Springer, Berlin.

Didymus, J. M., P. Oliver, S. Mann, A. L. DeVries, P. V. Hauschka, and P. Westbroek. 1993. Influence of low-molecular weight and macromolecular organic additives on the morphology of calcium carbonate. *J. Chem. Soc. Faraday Trans.* **89:** 2891–2900.

Dillaman, R. M., and S. E. Ford. 1982. Measurement of calcium carbonate deposition in molluscs by controlled etching of radioactively labeled shells. *Mar. Biol.* **66:** 133–143.

Erben, H. K., and N. Watabe. 1974. Crystal formation and growth in bivalve nacre. *Nature* **248:** 128–130.

Fallini, G., S. Albeck, S. Weiner, and L. Addadi. 1996. Control of aragonite or calcite polymorphism by mollusk shell macromolecules. *Science* **271:** 67–69.

Fincham, A. G., J. Moradian-Oldak, J. P. Simmer, P. Sarte, E. C. Lau, T. Diekwisch, and H. C. Slavkin. 1994. Self-assembly of a recombinant amelogenin protein generates supramolecular structures. *J. Struct. Biol.* **112:** 103–109.

Fincham, A. G., J. Moradian-Oldak, and H. C. Slavkin. 1995. Evidence for amelogenin "nanospheres" as functional components of secretory-stage enamel matrix. *J. Struct. Biol.* **115:** 50–59.

Fincham, A. G., J. Moradian-Oldak, and J. P. Simmer. 1999. The structural biology of the developing dental enamel matrix. *J. Struct. Biol.* **126:** 270–299.

Galtsoff, P. S. 1964. The American oyster *Crassostrea virginica* Gmelin. *Fish. Bull.* **64:** 1–480.

Giles, R., S. Manne, S. Mann, D. E. Morse, G. D. Stucky, and P. K. Hansma. 1995. Inorganic overgrowth of aragonite on molluscan nacre examined by atomic force microscopy. *Biol. Bull.* **188:** 8–15.

Gower, L. A., and D. A. Tirrell. 1998. Calcium carbonate films and helices grown in solutions of poly(aspartate). *J. Cryst. Growth* **191:** 153–160.

Heuer, A. H., D. J. Fink, V. J. Laraia, J. L. Arias, P. D. Calvert, K. Kendall, G. L. Messing, P. C. Rieke, D. H. Thompson, A. P. Wheeler, A. Veis, and A. I. Caplan. 1992. Innovative materials processing strategies: a biomimetic approach. *Science* **255:** 1098–1105.

Low, K. C. 1990. Adsorption of oyster shell matrix and its peptide analogs onto calcium carbonate: mechanisms of inhibition of crystal growth. Thesis, University of South Alabama, Mobile. 75 pp.

Lowenstam, H. A., and S. Weiner. 1989. *On Biomineralization.* Oxford University Press, New York.

Mann, S., ed. 1996. *Biomimetic Approaches in Materials Science,* VCH Publishers, New York.

Mann, S., J. M. Didymus, N. P. Sanderson, B. R. Heywood, and E. J. A. Samper. 1990. Morphological influence of functionalized and nonfunctionalized α, Ω-dicarboxylates on calcite crystallization. *J. Chem. Soc. Faraday Trans.* **86:** 1873–1880.

Marsh, M. E. 1986. Biomineralization in the presence of calcium-binding phosphoprotein particles. *J. Exp. Zool.* **239:** 207–220.

Marsh, M. E. 1989a. Self-association of calcium and magnesium complexes of dentin phosphophoryn. *Biochemistry* **28:** 339–345.

Marsh, M. E. 1989b. Binding of calcium and phosphate ions to dentin phosphophoryn. *Biochemistry* **28:** 346–352.

Marsh, M. E. 1994. Polyanions and biomineralization. *Bull. Inst. Oceanogr. (Monaco)* **14(1):** 121–128.

Marsh, M. E., and R. L. Sass. 1983. Calcium-binding phosphoprotein particles in the extrapallial fluid and innermost shell lamella of clams. *J. Exp. Zool.* **226:** 193–203.

Marsh, M. E., and R. L. Sass. 1984. Phosphoprotein particles: calcium and inorganic phosphate binding structures. *Biochemistry* **23:** 1448–1456.

Marsh, M. E., and R. L. Sass. 1985. Distribution and characterization of mineral-binding phosphoprotein particles in bivalvia. *J. Exp. Zool.* **234:** 237–242.

Misogianes, M., and N. D. Chasteen. 1979. A chemical and spectral characterization of the extrapallial fluid of *Mytilus edulis*. *Anal. Biochem.* **100:** 324–334.

Nair, P. S., and W. E. Robinson. 1998. Calcium speciation and exchange between blood and extrapallial fluid of the quahog *Mercenaria mercenaria* (L.). *Biol. Bull.* **195:** 43–51.

Okazaki, K., and S. Inoué. 1976. Crystal property of the larval sea urchin spicule. *Dev. Growth Differ.* **18:** 413–434.

Okazaki, K., R. M. Dillaman, and K. M. Wilbur. 1981. Crystalline axes of the spine and test of the sea urchin *Strongylocentrotus purpuratus:* determination by crystal etching and decoration. *Biol. Bull.* **161:** 402–415.

Paine, R. T. 1964. Ash and calorie determinations of sponge and opisthobranch tissues. *Ecology* **45:** 384–387.

Price, T. J., G. W. Thayer, M. W. LaCroix, and G. P. Montgomery. 1976. The organic content of shells and soft tissues of selected estuarine gastropods and pelecypods. *Proc. Natl. Shellfish. Assoc.* **65:** 26–31.

Runnegar, B. 1984. Crystallography of the foliated calcite shell layers of bivalve molluscs. *Alcheringa* **8:** 273–290.

Sarikaya, M., J. Liu, and I. A. Aksay. 1995. Nacre: properties, crystallography, and formation. Pp. 35–90 in *Biomimetics: Design and Processing of Materials,* M. Sarikaya and I. A. Aksay, eds. American Institute of Physics, New York.

Sikes, C. S., and A. P. Wheeler. 1986. The organic matrix from oyster shell as a regulator of calcification *in vivo*. *Biol. Bull.* **170:** 494–505.

Sikes, C. S., and A. Wierzbicki. 1995. Mechanisms of regulation of crystal growth in selected biological systems. Pp. 183–206 in *Mineral Scale Formation and Inhibition,* Z. Amjad, ed. Plenum Press, New York.

Sikes, C. S., and A. Wierzbicki. 1996. Polyamino acids as antiscalants, dispersants, antifreezes, and absorbent gelling materials. Pp. 249–278 in *Biomimetic Approaches in Materials Science,* S. Mann, ed. VCH Publishers, New York.

Sikes, C. S., A. P. Wheeler, A. Wierzbicki, R. M. Dillaman, and L. De Luca. 1998. Oyster shell protein and atomic force microscopy of oyster shell folia. *Biol. Bull* **194:** 304–316.

Simkiss, K. 1994. Amorphous minerals in biology. *Bull. Inst. Oceanogr. (Monaco)* **14(1):** 49–54.

Simkiss, K., and K. M. Wilbur. 1989. *Biomineralization.* Academic Press, San Diego, CA.

Stupp, S. I., and P. V. Braun. 1997. Molecular manipulation of microstructures: biomaterials, ceramics, and semiconductors. *Science* **277:** 1242–1248.

Taylor, J. D., W. J. Kennedy, and A. Hall. 1969. The shell structure and mineralogy of the bivalvia. Introduction. Nuculacea-Trigonacea. *Bull. Br. Mus. (Nat. Hist.) Zool., Supplement* **3:** 1–125, plates 1–29.

Tsujii, T., G. D. Sharp, and K. M. Wilbur. 1958. Studies on shell formation. VII. The submicroscopic structure of the oyster *Crassostrea virginica*. *J. Biophys. Biochem. Cytol.* **4:** 275–279.

Wada, K. 1963. Studies on the mineralization of the calcified tissue in molluscs. VI. Crystal structure of the calcite grown on the inner surface of calcitostracum. *J. Electron Microsc.* **12:** 224–227.

Wada, K. 1968. Spiral growth of calcitostracum. *Nature* **219:** 62.

Wada, K. 1990. Initiation of mineralization in bivalve molluscs. Pp. 79–92 in *The Mechanisms of Biomineralization in Animals and Plants,* M. Omori and N. Watabe, eds. Tokai University Press, Tokyo.

Wada, K. and T. Fujinuki. 1976. Biomineralization in bivalve molluscs with emphasis on the chemical composition of the extrapallial fluid. Pp. 175–190 in *The Mechanisms of Mineralization in the Invertebrates and Plants,* N. Watabe and K. M. Wilbur, eds. University of South Carolina Press, Columbia.

Watabe, N. 1965. Studies on shell formation. XI. Crystal-matrix relationships in the inner layers of mollusk shells. *J. Ultrastruct. Res.* **12:** 351–370.

Watabe, N. 1974. Crystal growth of calcium carbonate in biological systems. *J. Cryst. Growth* **24/25:** 116–122.

Watabe, N. 1981. Crystal growth of calcium carbonate in the invertebrates. *Prog. Cryst. Growth Charact.* **4:** 99–147.

Watabe, N., and K. M. Wilbur. 1961. Studies on shell formation. IX. An electron microscope study of crystal layer formation in the oyster. *J. Biophys. Biochem. Cytol.* **9:** 761–771.

Watabe, N., D. G. Sharp, and K. M. Wilbur. 1958. Studies on shell formation. VIII. Electron microscopy of crystal growth of the nacreous layer of the oyster *Crassostrea virginica*. *J. Biophys. Biochem. Cytol.* **4:** 281–284, plates 152–156.

Weiner, S., and L. Addadi. 1997. Design strategies in mineralized biological materials. *J. Mater. Chem.* **7:** 689–702.

Wen, H. B., J. Moradian-Oldak, W. Leung, P. Bringas Jr., and A. G. Fincham. 1999. Microstructures of an amelogenin gel matrix. *J. Struct. Biol.* **126:** 42–51.

Wheeler, A. P., and L. P. Koskan. 1993. Large scale thermally synthesized polyaspartate as a biodegradable substitute in polymer applications. *Mater. Res. Soc. Symp. Proc.* **292:** 277–283.

Wheeler, A. P., and C. S. Sikes. 1989. Matrix-crystal interactions in $CaCO_3$ biomineralization. Pp. 95–133 in *Biomineralization: Chemical and Biochemical Perspectives,* S. Mann, J. Webb, and R. J. P. Williams, eds. VCH Publishers, Weinheim, Germany.

Wheeler, A. P., and K. M. Wilbur. 1977. Shell growth in the scallop

Argopecten irradi... ...ay). II. Processes of shell growth. *J. Molluscan Stud.* **43:** 155–16...

Wheeler, A. P., P... Blackwelder, and K. M. Wilbur. 1975. Shell growth in th... *Argopecten irradians*. I. Isotope incorporation with reference ... normal growth. *Biol. Bull.* **148:** 472–482.

Wheeler, A. P., K. W. Rusenko, D. M. Swift, and C. S. Sikes. 1988. Regulat... of $CaCO_3$ formation by fractions of oyster shell matrix. *Mar. Bio...* **98:** 71–80.

Wheeler, A. P., K. C. Low, and C. S. Sikes. 1991. $CaCO_3$ crystal-bindi... g properties of peptides and their influence on crystal growth. Pp. 72–84 in *Surface Reactive Peptides and Polymers: Discovery and Commercialization*, Symposium Series 444, C. S. Sikes and A. P. Wheeler, eds. ACS Books, Washington, DC.

Wierzbicki, A., C. S. Sikes, B. Drake, and J. Madura. 1994. Atomic force microscopy and molecular modeling of protein and peptide binding to calcite. *Calcif. Tissue Int.* **54:** 133–141.

Wilbur, K. M., and A. M. Bernhardt. 1984. Effects of amino acids, magnesium, and molluscan extrapallial fluid on crystallization of calcium carbonate: *in vitro* experiments. *Biol. Bull.* **166:** 251–259.

Wilbur, K. M., and L. H. Jodrey. 1952. Studies on shell formation. I. Measurement of the rate of shell formation using Ca^{45}. *Biol. Bull.* **103:** 269–276.